PHYSICAL REVIEW B **79**, 014427 (2009)

Local and average structures of the spin-glass pyrochlore $Y_2Mo_2O_7$ from neutron diffraction and neutron pair distribution function analysis

J. E. Greedan,[1] Delphine Gout,[2] A. D. Lozano-Gorrin,[1] Shahab Derahkshan,[1] Th. Proffen,[3] H.-J. Kim,[3] E. Božin,[4] and S. J. L. Billinge[4]

[1]*Department of Chemistry and Brockhouse Institute for Materials Research, McMaster University, Hamilton, Canada L8S 4M1*

[2]*Jülich Center for Neutron Science–SNS, Forschungszentrum Jülich, 52425 Jülich, Germany and Oak Ridge National Laboratory, P.O. Box 2008, Oak Ridge, Tennessee 38371, USA*

[3]*Lujan Neutron Scattering Center, Los Alamos National Laboratory, Los Alamos, New Mexico 87545, USA*

[4]*Department of Applied Physics and Applied Mathematics, Columbia University, New York, New York 10027, USA and Condensed Matter and Materials Science Department, Brookhaven National Laboratory, Upton, New York 11973, USA*

(Received 18 November 2008; revised manuscript received 11 December 2008; published 21 January 2009)

The observation of canonical spin-glass behavior in the pyrochlore oxide $Y_2Mo_2O_7$ has been a subject of considerable interest as the original structural studies were interpreted in terms of a well-ordered crystallographic model. It is widely held that the stabilization of the spin-glass state requires some level of positional disorder along with frustration. Recent reports from local probe measurements, extended x-ray-absorption fine structure (EXAFS) and ^{89}Y NMR, have been interpreted in terms of disorder involving the Mo-Mo distances (EXAFS) and multiple Y sites (NMR). This work reports results from temperature-dependent (15–300 K) neutron diffraction (ND) and neutron pair distribution function studies which can provide from the same data set information on both the average and local structures. The principal findings are that: (1) there is no crystallographic phase transition over the temperature region studied within the resolution of the ND data; (2) the diffraction data are well fitted using a fully ordered model but with large and anisotropic displacement parameters for three of the four atomic sites; (3) the pairwise real-space correlation function $G(r)$ shows clear evidence that the principal source of disorder is associated with the Y-O1 atom pairs rather than the Mo-Mo pairs, in disagreement with the interpretation of the EXAFS results; (4) fits to the $G(r)$ improve significantly when anisotropic displacements for all sites are included; (5) inclusion of a split-site position parameter for O1 improves, slightly, both the $G(r)$ fits and the Rietveld fits to the ND data; and (6) for all models the fits become worse as the temperature decreases and as the fitting range decreases. These results are qualitatively consistent with the ^{89}Y NMR observations and perhaps recent muon-spin-relaxation studies. The issue of static versus dynamic disorder is not resolved, definitively. An estimate of the distribution of exchange constants due to the disorder is made using spin-dimer analysis and compared with the Saunders-Chalker model for the generation of spin-glass behavior from "weak" disorder on geometrically frustrated lattices.

DOI: 10.1103/PhysRevB.79.014427 PACS number(s): 75.50.Lk, 61.05.fm

I. INTRODUCTION

Geometrically frustrated materials with nearest-neighbor antiferromagnetic (AF) constraints can exhibit a variety of ground states including long-range but complex-order, spin-liquid and spin-glass (SG) behaviors. If the constraints are ferromagnetic and accompanied by strong axial anisotropy, the spin-ice state may be stabilized. Materials with the pyrochlore structure, mostly oxides, have been central to investigations of such phenomena and the voluminous literature has been reviewed recently.[1] Among the known pyrochlore oxides for which there is no obvious compositional disorder, there are only a few examples of the SG ground state. The best studied of these is $Y_2Mo_2O_7$, which was first tentatively characterized as a spin glass with $T_f=22$ K on the basis of low-temperature dc susceptibility results in 1986,[2] although high-temperature data had been reported as early as 1975.[3,4] Subsequent work has established that $Y_2Mo_2O_7$ does indeed behave as a nearly ideal spin glass from nonlinear susceptibility, heat-capacity, ac susceptibility, elastic and inelastic neutron-scattering, muon-spin-relaxation, and neutron spin-echo data, for example.[5–11] There appears to be little doubt that $Y_2Mo_2O_7$ is a spin glass; indeed the critical exponents extracted from the analysis of the nonlinear dc susceptibility agree well with those found in classical disordered spin-glass systems.[5] It is a widely held tenet that in order for the SG state to be stable, both frustration and positional disorder must be present, simultaneously. This is certainly the case in the classical spin glasses such as dilute solid solutions of iron in gold, Fe_xAu_{1-x}, with $x\sim0.05$, where the randomness of the Fe sites and the Ruderman-Kittel-Kasuya-Yosida (RKKY) exchange mechanism combine to produce the spin-glass state. Another class of spin glasses can be obtained by dilution of the magnetic sites of an antiferromagnetic or a ferromagnetic insulator with a diamagnetic substituent. Among many examples are the antiferromagnets $Fe_xZn_{1-x}F_2$ and $Fe_xMg_{1-x}TiO_3$, where a SG state obtains for x values near the percolation threshold.[12,13] In other cases, $Eu_xSr_{1-x}S$, for example, a SG state emerges for x values ($x\sim0.5$) well above the percolation limit ($x\sim0.2$).[14] Here, competing nearest-neighbor ferromagnetic and next-nearest-neighbor antiferromagnetic interactions are key factors. In all of the above examples, significant levels of positional disorder induce magnetic frustration in the relevant systems. For the pyrochlore oxides in which dilution effects are clearly not present, another mechanism must be operable.

TABLE I. Description of the $A_2B_2O_7$ pyrochlore structure in $Fd3m$.

Atom	Wyckoff site	Point symmetry	Minimal coordinates
A	16*d*	−3*m*	1/2 1/2 1/2
B	16*c*	−3*m*	0 0 0
O1	48*f*	*mm*	*x* 1/8 1/8
O2	8*b*	−43*m*	3/8 3/8 3/8

Before proceeding further, it is highly relevant to consider the existing structural evidence from neutron diffraction (ND) which measures, of course, the average structure. The formal description of the pyrochlore structure for materials, mostly oxides with composition $A_2B_2O_7$, is within space group $Fd3m$ as shown in Table I. There are four occupied positions, the choice with *A* in 16*d*, *B* in 16*c*, O1 in 48*f*, and O2 in 8*b* is now considered standard, although in earlier literature other origins have been used.[15]

In the original neutron powder diffraction study, the fully ordered model was refined for $Y_2Mo_2O_7$ with Y in 16*d*, Mo in 16*c*, and O2 in 8*b*, and the lone positional parameter for O1 in 48*f* was found to be $x=0.3382(1)$ with the cubic lattice constant $a_0=10.230(1)$ Å.[16] Some disorder models involving O2 were explored but these gave no improvement on the ideal model. Anisotropic displacement parameters were refined for the Y site and these gave an ellipsoid flattened normal to the local axis which is a ⟨111⟩-type direction within the unit cell. All interatomic distances were reasonable for the fully ordered model, being in excellent agreement with the sum of the effective ionic radii.

Of course all real materials will contain various types of defects, generally at low levels. Concentrations can be difficult to measure but recent computational results for pyrochlore oxides suggest values on the order of 1%.[17] For $Y_2Mo_2O_7$ the calculated antisite (Y/Mo exchange) defect level is 1.1% and the oxygen vacancy level is 0.4%. Are such defect concentrations sufficient to induce spin-glass behavior? This seems somewhat unlikely on the basis that only a few nominally stoichiometric pyrochlores are actually spin glasses and the defect levels are calculated to be similar for all oxide materials of this structure type. One known case for which spin-glass behavior results from very low levels of substitutional disorder is that of Cd-doped $ZnCr_2O_4$.[18] Here, Cd substitution for Zn at the 3% level is sufficient to destroy the Néel order in $ZnCr_2O_4$. For this material, the Cr^{3+} sublattice has pyrochlore topology and in the pure phase undergoes a tetragonal distortion which presumably lifts the ground-state degeneracy and selects an AF long-range-order (LRO) ground state with $T_N=14$ K. It is argued that the large size mismatch between Cd^{2+} and Zn^{2+}, 0.78 Å versus 0.60 Å, respectively,[19] induces random strains which, in the presence of strong magnetoelastic coupling, can result in the spin-glass ground state. Interestingly, substitution of diamagnetic Ga^{3+} on the Cr^{3+} sites is much less effective, with the SG state appearing only at concentrations approaching 20% Ga. Ga^{3+} and Cr^{3+} have nearly identical radii for sixfold coordination, 0.62 Å.

Saunders and Chalker[20] attempted to explain the occurrence of the SG ground state in geometrically frustrated magnets with "weak" disorder levels. In this approach, weak disorder is defined as $\Delta \ll J$, where J is the average exchange constant and Δ is its fluctuation. The model considered is the classical Heisenberg antiferromagnet with near-neighbor exchange on a pyrochlore lattice. The central results are that the spin-glass correlation function is finite at large distances for a range of Δ and that the spin-freezing temperature $T_f \propto \Delta$ but is independent of J. Quantitative application of these ideas to actual systems is not straightforward as the relationship of $\Delta(J)$ to a specific disorder or defect mechanism will be complex and perhaps not easily established.

Nonetheless, it is still important to identify the nature of the disorder in materials such as $Y_2Mo_2O_7$ in a first effort to understand its unique behavior. Recently, there have been two studies, both involving local probes, which provide some evidence for disorder in this material. Extended x-ray-absorption fine structure (EXAFS) data for both Mo and Y edges have been interpreted in terms of a large static variance in the Mo-Mo distances, $\Delta^2=0.026(5)$ Å^2, which is ~10 times larger than the variances found for Mo-O1, Mo-Y, and Y-Y distances, for example.[21] This implies a fluctuation in the Mo-Mo bond distance of 0.16(2) Å, which is ~4% of the equilibrium Mo-Mo distance. It has been widely suggested that this disorder level may explain the spin-glass ground state but no quantitative link has been established. In another study ^{89}Y NMR data show a large number of resonances when $Y_2Mo_2O_7$ is cooled below 200 K.[22] This can be interpreted as evidence for a local multiplicity of Y sites, in contrast to the average structure value of one. As the Weiss temperature for this material is −200 K, the suggestion was made that the disorder was somehow "frustration driven" but no evidence has yet been presented for a true phase transition as seen for the case of $ZnCr_2O_4$ described above. Subsequent muon spin relaxation (μSR) studies in applied fields have attempted to measure the distribution of local magnetic fields seen by the muon in $Y_2Mo_2O_7$ which was equated with the distribution in exchange constants.[23] It was concluded that this distribution increases rapidly below 40 K. Another study, not on $Y_2Mo_2O_7$ but instead on isostructural $Yb_2Mo_2O_7$, is worth mentioning. ^{170}Yb Mössbauer-effect data must be interpreted in terms of a distribution of electric field gradients at the Yb site, suggesting some type of disorder on the *A* site.[24] Interestingly, a similar disorder but of lesser magnitude is noted for ferromagnetic $Gd_2Mo_2O_7$.

There is in these studies the usual dichotomy between the information obtained from diffraction probes which determine the average structure and the local probes where the structural information is restricted to very short length scales, often that between nearest neighbors. It is, thus, challenging to reconcile the two types of data to provide a consistent interpretation. Ideally, one would like to use a method which could, from the same data set, provide information on both the local and average structure. The neutron pair distribution function (NPDF) method meets this criterion.[25] In this approach diffraction data, $S(Q)$, are collected to very large momentum transfers, $Q \sim 30-40$ Å^{-1}. Fourier transformation of suitably normalized data can then yield the real-space pairwise distribution function, $G(r)$, from which local structure information can be extracted. Of course the same $S(Q)$ data can be analyzed using conventional Rietveld crystallo-

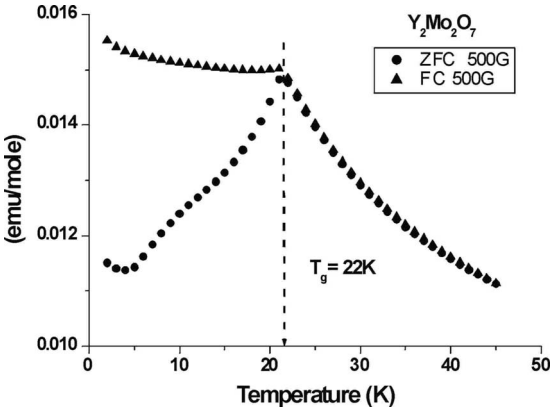

FIG. 1. Low-temperature dc magnetic susceptibility for the $Y_2Mo_2O_7$ sample used in these studies.

graphic tools to yield the average structure. Recent advances in instrumentation, especially at spallation neutron sources, and corresponding developments in data analysis codes have now made this technique more widely accessible.[26,27] In the following, ND and NPDF data are used to characterize both the average and local structure of $Y_2Mo_2O_7$ over a wide temperature range, 15–300 K, which includes those for which the EXAFS and NMR studies were done and extending well into the spin-glass regime.

II. EXPERIMENTAL

A. Sample preparation and characterization

$Y_2Mo_2O_7$ was prepared from starting materials, MoO_2 (99.9%) and Y_2O_3 (99.99%). Y_2O_3 was fired at 1000 °C for 8 h. before weighing. The mixture was ground and mixed well in a mortar and pestle, then pelletized and fired at 1300 °C for 48 h in a buffer gas mixture $CO/CO_2=1$ as described in a previous report.[28] The material was determined to be single phase from x-ray powder diffraction using a Guinier-Hägg camera. Magnetic-susceptibility data were collected using a Quantum Design superconducting quantum interference device (SQUID) magnetometer.

B. Neutron scattering and data handling

Neutron-scattering data were collected on the instrument NPDF at the M. Lujan Jr. Center for Neutron Scattering at the Los Alamos Neutron Science Center. This instrument has been described elsewhere.[26] The sample of ~5 g was contained in a vanadium can which was placed in a Displex closed-cycle refrigerator. Background corrections were determined by measuring the empty sample chamber, empty Displex, and empty vanadium sample can. Detector efficiency was normalized by measuring a vanadium rod. Data were collected to a limit of $Q=45$ Å^{-1} at several temperatures between 300 and 15 K. Data for neutron diffraction analysis were obtained by truncating the data at $Q=9$ Å^{-1}, while for PDF analysis, the truncation limit was taken as $Q=35$ Å^{-1} based on inspection of the noise level in the data. Standard data corrections were carried out using $PDF_{get}N$.[25] Corrected data were normalized by the total scattering cross section of the sample to yield the total scattering structure factor $S(Q)$, where Q is the scattering or momentum transfer vector, $Q=4\pi \sin\theta/\lambda$. The $G(r)$ was obtained by a sine Fourier transform according to

$$G(r) = 4\pi r[\rho(r) - \rho_0] = 2/\pi \int_0^\infty Q[S(Q) - 1]\sin(Qr)dQ,$$

where $\rho(r)$ is the atomic pair density and ρ_0 is the average atomic number density. The ND data were refined using the GSAS package and the refinements of $G(r)$ were done with PDFFIT and PDFGUI, the latter permitting the refinement of anisotropic atomic displacement factors (ADFs).[27]

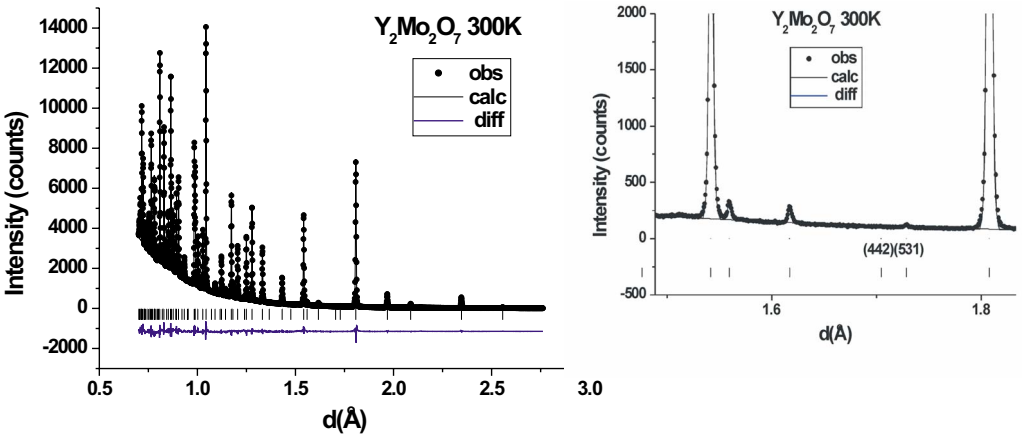

FIG. 2. (Color online) (Left) A Rietveld fit for the neutron diffraction data for $Y_2Mo_2O_7$ at 300 K on the fully ordered model using ADFs for all atoms. $R_{wp}=4.01\%$. The black circles are the data, the solid line is the model, and the lower curve is the difference plot. Bragg-peak positions are shown by the vertical tic marks. (Right) The region including the 442 reflection position showing the absence of this reflection. The very weak but allowed 531 reflection is also marked.

TABLE II. Rietveld refinement results with anisotropic ADFs for $Y_2Mo_2O_7$ at various temperatures.

T (K)	a_0 (Å)	x(O1)	R_{wp}
300	10.23025(2)	0.337689(29)	0.0407
225	10.22129(2)	0.33788(4)	0.0468
200	10.21859(2)	0.337811(33)	0.0419
150	10.21352(2)	0.337852(30)	0.0444
100	10.21014(2)	0.338031(33)	0.0498
50	10.20828(2)	0.338047(31)	0.0480
25	10.20759(2)	0.338071(32)	0.0492
20	10.20759(2)	0.338080(32)	0.0487
15	10.20753(2)	0.338088(32)	0.0482

III. RESULTS AND DISCUSSION

A. Magnetic characterization

Magnetic-susceptibility data taken at 0.05 T are shown in Fig. 1. Note the divergence between the data collected in zero-field-cooled and field-cooled modes at 22 K which can be taken as the spin-glass freezing temperature T_F. These data are consistent with several other determinations shown in the literature and indicate that this sample is equivalent in terms of magnetic properties to typical samples of $Y_2Mo_2O_7$.

B. Neutron diffraction: The average structure

The only structural study previously published[16] was based on data taken at a low-flux reactor-based source with modest resolution, so it is of considerable interest to analyze data of superior resolution and extended Q range as afforded here. Initially, the data sets at each temperature were refined using both isotropic and anisotropic ADFs on the fully ordered model. A typical result is shown in Fig. 2, left panel, from which it is clear that the fit is excellent. Figure 2, right panel, demonstrates the absence of the 442 reflection, the significance of which is discussed later in this section. The refinement results are listed in Tables II–IV for anisotropic ADFs and the temperature dependence of the anisotropic ADFs is shown in Fig. 3, left panel, while the ellipsoids are indicated in Fig. 3, right panel.

First the anisotropic refinement results at 300 K can be compared directly with those for other pyrochlores, for example, $Y_2Sn_2O_7$, obtained also from neutron powder data as shown in Table V.[29] These results were obtained at a reactor source to $Q_{max}=8.1$ Å^{-1} comparable to those of the present work for which $Q_{max}=9.1$ Å^{-1}. The effective radii for Sn^{4+} (0.69 Å) and Mo^{4+} (0.65 Å) are comparable.[19]

Note that, except for the O2 site, the diagonal displacement factors for B=Mo are significantly larger, by factor of 2 or 3, than those for the B=Sn pyrochlore. The shapes of the ellipsoids at the B site are different as well, with negative off-diagonal values for B=Sn which are positive for B=Mo. Thus, the Sn ellipsoid is a disklike slightly flattened sphere, while for B=Mo, it is an elongated cigar shape (Fig. 3, right panel). Considering relative magnitudes among ADFs for $Y_2Mo_2O_7$, U_{11}(O1) is the largest of all by nearly a factor of 2. Examination of the temperature dependence of the displacements (Fig. 3, left panel) indicates normal behavior for most, but U_{11} for O1 remains very large and U_{11} for Mo shows nearly no temperature dependence. Thus, in spite of the excellent apparent fit of the fully ordered model to the data, it is clear that all of the atomic displacement factors are large and show considerable anisotropy except of course for O2, for which the site symmetry constrains the ellipsoid to be spherical. Before leaving this discussion, it is worth noting that the 442 reflection, which has been linked with static atomic displacements in pyrochlores, is not observed in the neutron data (Fig. 2, right panel). For example, pyrochlores with so-called lone pair active ions on the A site, e.g., $Bi_2Ti_2O_7$ or $Sn_2Ta_2O_7$, for which a clear static distortion has been demonstrated, always show a 442 reflection.[30,31] In these cases the lone pair ion is disordered over the 96g sites and O2 is partially distributed over 32e. The origin of this correlation is that additional systematic absences arise in $Fd3m$ with isotropic atoms in Wyckoff sites $a-d$ and f which forbid 442 but for atoms in any other site these additional extinctions do not hold. Apparently, anisotropic atoms in these special sites also allow 442 in principle but in the case of $Y_2Mo_2O_7$, it is absent in spite of large-amplitude anisotropic behavior at all of these sites except of course 8b. Finally, the absence of 442 argues against disorder of O2 in 32e.

TABLE III. Anisotropic ADFs $U_{ij}\times 10^2$ Å^2 for $Y_2Mo_2O_7$ at various temperatures.

T (K)	$U_{11}(Y)$	$U_{12}(Y)$	U_{11}(Mo)	U_{12}(Mo)	U_{11}(O1)	U_{22}(O1)	U_{23}(O1)	U_{11}(O2)
300	0.856(9)	−0.224(9)	1.14(1)	0.61(1)	1.85(2)	0.96(1)	0.16(1)	0.56(2)
225	0.648(9)	−0.19(1)	0.99(1)	0.69(2)	1.64(2)	0.70(1)	0.16(2)	0.35(2)
200	0.722(8)	−0.18(1)	1.15(1)	0.75(2)	1.72(2)	0.82(1)	0.11(1)	0.46(2)
150	0.732(7)	−0.162(9)	1.27(1)	0.80(1)	1.73(2)	0.868(9)	0.06(1)	0.50(2)
100	0.511(8)	−0.16(1)	1.11(1)	0.81(2)	1.45(2)	0.677(9)	0.03(1)	0.34(2)
50	0.497(7)	−0.130(9)	1.14(1)	0.84(2)	1.48(2)	0.680(9)	0.03(1)	0.35(2)
25	0.491(7)	−0.14(1)	1.14(1)	0.83(2)	1.47(2)	0.691(9)	0.03(1)	0.35(2)
20	0.471(7)	−0.140(9)	1.12(1)	0.82(2)	1.44(2)	0.667(9)	0.03(1)	0.35(2)
15	0.471(7)	−0.136(9)	1.11(1)	0.83(2)	1.45(2)	0.66(1)	0.03(1)	0.32(2)

TABLE IV. Selected interatomic distances (Å) for $Y_2Mo_2O_7$ from Rietveld refinements.

T (K)	Y-O1	Y-O2	Mo-O1	Y-Y/Mo-Mo
300	2.4552(2)	2.21491(1)	2.0187(1)	3.61694(1)
225	2.4517(3)	2.21297(1)	2.0178(2)	3.61377(1)
200	2.4515(2)	2.21239(1)	2.0170(2)	3.62182(1)
150	2.4500(2)	2.21129(1)	2.0162(1)	3.61102(1)
100	2.4480(2)	2.21056(1)	2.0163(2)	3.60983(1)
50	2.4474(2)	2.21016(1)	2.0160(2)	3.60917(1)
25	2.4471(2)	2.21001(1)	2.0160(2)	3.60893(1)
20	2.4470(2)	2.21001(1)	2.0160(2)	3.60893(1)
15	2.4469(2)	2.20999(1)	2.0161(2)	3.60891(1)

The average structure data can also be used to examine the possibility of a crystallographic phase transition, frustration driven or otherwise, within the temperature range investigated. For example, the data of Fig. 3 show some scatter but no discontinuity in the ADFs as the temperature is lowered, nor is there any other discontinuity such as in the cell constant or the x(O1). Figure 4 shows a comparison of data from the 148° backscattering detector bank for 300 and 20 K. Within the resolution of these data, $\Delta d/d \sim 1.5 \times 10^{-3}$, there is no evidence for new reflections or peak splitting or broadening which would signal a crystallographic phase transition to a lower symmetry as the temperature decreases to below the observed T_F.

C. Pair distribution function analysis: The local structure

The $G(r)$ shows sharp features out to quite long distances, indicating a high degree of crystallinity for the sample. In these studies a $r_{max}=20$ Å has been chosen for fitting and is displayed in Fig. 6. The weak ripples below about 2 Å are unphysical, coming from errors in the data analysis.[32] They are small, indicating the good quality of the data, and are insignificant in the physical region of the PDF above 1.8 Å. There is merit in examining the region of small r which includes the nearest-neighbor pairwise distances for this material. Figure 5 displays the $G(r)$ out to 3.8 Å, showing six

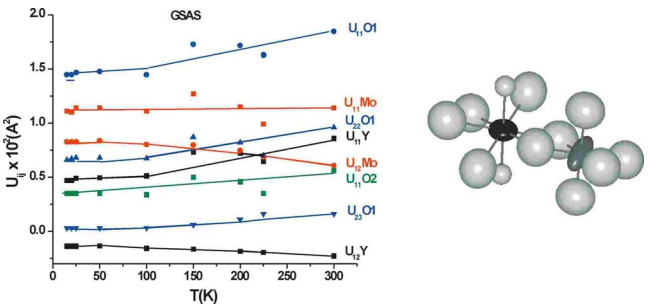

FIG. 3. (Color online) (Right) Temperature dependence of the anisotropic displacement factors for $Y_2Mo_2O_7$. The lines are guides for the eyes. (Left) The ADF ellipsoids at 300 K. Y is black, Mo is dark gray, O1 is large and white, and O2 is small and white.

TABLE V. Comparison of anisotropic displacement factors (10^{-2} Å^2) for $Y_2B_2O_7$ pyrochlores at 300 K; B=Sn,Mo.

Parameter (Site)	B=Sn	B=Mo
$U_{11}=U_{22}=U_{33}$ (Y)	0.54(2)	0.856(9)
$U_{12}=U_{13}=U_{23}$ (Y)	−0.09(2)	−0.224(9)
$U_{11}=U_{22}=U_{33}$ (Sn,Mo)	0.27(2)	1.14(1)
$U_{12}=U_{13}=U_{23}$ (Sn,Mo)	−0.03(2)	0.61(1)
U_{11} (O1)	0.64(3)	1.85(2)
$U_{22}=U_{33}$ (O1)	0.56(2)	0.96(1)
U_{23} (O1)	0.23(2)	0.16(1)
$U_{11}=U_{22}=U_{33}$ (O2)	0.49(4)	0.56(2)

resolved peaks, each of which can be assigned unambiguously as indicated by comparison of the peak maxima with the interatomic distances refined from the Rietveld analysis (Table IV).

Note that the peaks for Y-O1 and O1-O1 which correspond to a difference of 0.16 Å are sufficiently well resolved to be readily identified. At this stage it is of interest to compare the interpretation of the EXAFS data in terms of a static splitting of the Mo site with magnitude of ~0.16 Å directly to the $G(r)$. Unfortunately, due to the cubic symmetry, two atom pairs contribute to the peak at 3.62 Å, Y-Y and Mo-Mo, each involving six neighbors. The total intensity of a peak in the $G(r)$ is given by $I_{tot}=\Sigma_{ab}N_{ab}b_ab_b$, where N_{ab} is the number of contributing atom pairs and b_a and b_b are the scattering lengths of the atoms in the pair. The relative contribution of a given pair to the total peak intensity is thus $N_{ab}b_ab_b/I_{tot}$. On this basis the Mo-Mo pairs account for 41% of the peak intensity at 3.62 Å, a significant fraction. Note that there is no evidence for two observable peaks in the $G(r)$ at this distance. The EXAFS analysis found no unusual behavior of the Y-Y correlation, so in spite of the coincidence of the two atom pairs in the $G(r)$, one could expect to see Mo site splitting manifested in the form of discernable shoulders or at least a strong deviation from a Gaussian peak shape, which is also not evident. From another point of view, one can compare the relative widths of the Mo-O1 and Mo-Mo peaks between the $G(r)$ and the EXAFS fits. In the latter experiment the ratio of the variances, Δ^2, for Mo-Mo/Mo-O1 is given as ~11, which implies that the ratio of the peak widths should be ~3.3. Inspection of Fig. 5 shows that this is not observed; in fact the actual ratio is 1.5 at 300 K, which reduces to 1.1 at 15 K. Thus, the observed $G(r)$ does not appear to support a disorder model involving a split static Mo position of the magnitude needed to explain the EXAFS data. In addition one can compare the relative peak heights in the $G(r)$ data which should scale according to the equation given earlier, assuming a common peak width. Note that the Y-O1 ($x6$) peak is actually less intense than the Mo-O1 peak ($x6$) and even less intense than the Y-O2 peak ($x2$), whereas one would expect the relative peak height ratios to be 3/2.7/1 for the three atom pairs in the order listed. This indicates that, even without any fitting of the $G(r)$ data, attention is focused on the Y-O1 pairs as the principal origin of short-range disorder in this material. While the EXAFS data do

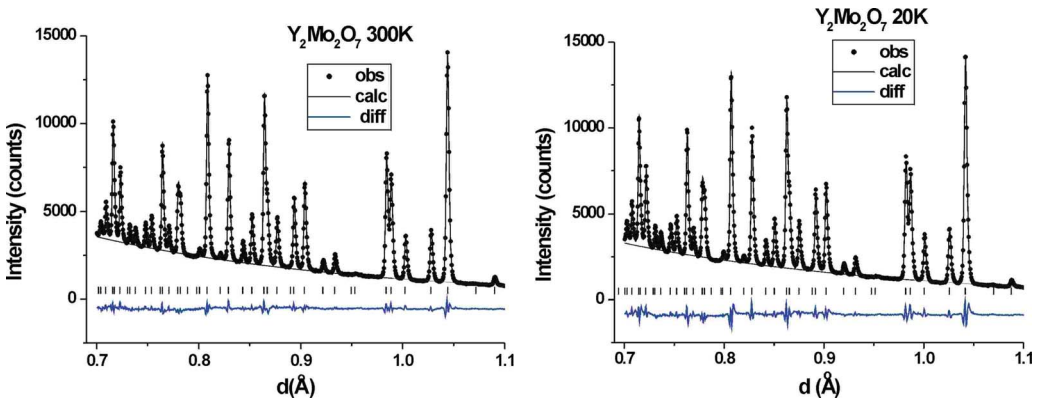

FIG. 4. (Color online) Comparison of neutron diffraction data at short d spacings for $Y_2Mo_2O_7$ at 300 K (left) and 20 K (right) showing the absence of a structural phase transition.

show anomalous behavior associated with the Mo-Mo pairs, this may be traced to the very large degree on anisotropy associated with the Mo ADF, but there is no clear evidence from the $G(r)$ for a static splitting. Of course much more definitive conclusions can be extracted from a detailed modeling of the NPDF data.

The $G(r)$ data were fitted using three models. The first involved the fully ordered model and isotropic ADFs, U_{iso}, for all atoms, and the results for 300 and 15 K are shown in Fig. 6. Clearly, the result at 300 K is poor with an agreement index $R_w=12\%$. Insight into the problems with this model is afforded by viewing the short-r regime, shown at the top right in Fig. 6. Here, as anticipated already, it is clear that the major area of poor fit involves the Y-O1 and O1-O1 sites. Clearly, the Y-O1 peak is strongly overestimated in the fit. While a difference peak occurs at Mo-Mo/Y-Y/Mo-Y, it is of the opposite sense, i.e., the data peak is actually sharper than the fitted peak, again a counterindication with respect to the EXAFS-derived model. Essentially the same situation is found at low temperature. Figure 6 bottom shows comparable data at 15 K, below T_f. Note that R_w is larger at 15 K, almost 16%. The data of Fig. 6 are not inconsistent with the large-amplitude anisotropic displacement parameters for the O1, Y, and Mo sites determined from the Rietveld analysis of the average structure.

Thus, the $G(r)$ data were fitted using anisotropic ADFs, U_{aniso}, for all atoms. The results at 300 and 15 K are shown in Fig. 7. Note first that R_w drops to 8% at 300 K and 10% at 15 K, both significant improvements to the fits. As seen in the short-r data, fits around the Y-O1 and Mo-Mo/Y-Y distances are much better. The total number of fitting parameters is now increased to 13 from 9 in the isotropic ADF model.

At this stage a static disorder model in which the O1 site was split was implemented. From the dimensions of the O1 ellipsoid, extreme x values of 0.329 and 0.346 were chosen as starting parameters and the O1 sites were divided into two groups of 24. This refinement in which all atoms were refined anisotropically showed a slight improvement in the fit at 300 K but results in the same R_w value as for the anisotropic ADF model at 15 K shown in Fig. 8. The number of refined parameters is now 16. The fitted values for x(O1) are 0.3305(12) and 0.3465(13).

Such a model can be checked using the diffraction data. To that end a refinement was attempted using a split O1 site in 48f. The starting x value was that from the fully ordered model. The results show that two independent x parameters can be refined with values of 0.3289(1) and 0.3466(1), very similar to those found from the PDF fit to the $G(r)$ data described above. However, it was not possible to refine simultaneously both the x values and the ADFs for each site. ADFs were refined separately, holding the x values constant, giving U_{11} and U_{22} values for the thermal ellipsoid of the O1 site which are now comparable, 0.0094(1) and 0.0089(1) Å^2, respectively. A major implication of the split-site model is that there are now two Y-O1 distances, 2.5165 and 2.3847 Å, with a mean value of 2.4556 Å and a standard deviation $\sigma=0.0609$, and two Mo-O1 distances, 1.9805 and 2.0606 Å, with a mean value of 2.023 Å and $\sigma=0.0376$. Such σ values would not result in resolvable features in the $G(r)$ as the observed full widths at half maximum (FWHMs) of the Mo-O peak and the Mo-Mo peak are 0.14 and 0.19 Å, respectively, at 300 K.

As has been noted previously, the R_w values for the fits to $G(r)$ increase for the same model as the temperature decreases. The global result for all models including the average structure is shown in Fig. 9. The common feature is that all agreement indices do increase with decreasing temperature but the behavior is different for each model. The average structure model shows the smallest effect with an increase from 4.07% at 300 K to 4.82% at 15 K, an overall change of 18%. The PDFFIT for the isotropic ADF model increases from 12.01% to 15.97%, a 33% change over the same range but

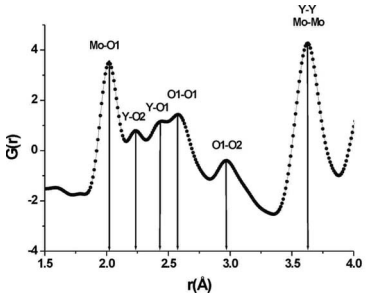

atom Pair	number	distance (Å)
Mo – O1	6	2.018
Y – O2	2	2.214
Y – O1	6	2.455
O1 – O1	2	2.613
O1 – O2	3	2.938
Mo – Mo Y – Y	12	3.616

FIG. 5. The short-r region of $G(r)$ for $Y_2Mo_2O_7$ at 300 K. Peak assignments are indicated.

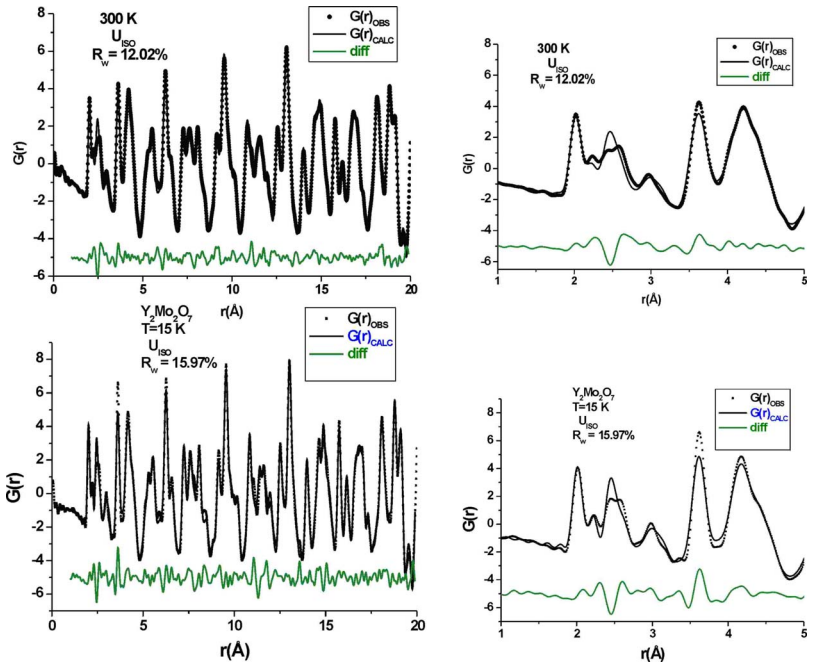

FIG. 6. (Color online) Fits to the $G(r)$ at 300 and 15 K: the fully ordered model with isotropic ADF. Top: 300 K; bottom: 15 K. Left: 0–20 Å; right: 1–5 Å.

R_w increases gradually to ~100 K and is then constant. For the other two models, there is a more discontinuous jump in R_w below 100 K for the all aniso models and below 50 K for the O1 split-site model. The overall changes are different, 22% for the former and 44% for the latter. Clearly, all models are less accurate at low temperature. These observations may be consistent with the recent μSR studies, mentioned above, which find a significant increase in the distribution of local fields below 40 K.[23]

Fits to the $G(r)$ were also carried out in which the range of r over which the fitting was done was varied. The minimum r value, $r_{\min}$, was fixed at 1 Å and $r_{\max}$ was increased systematically to 20 Å. The results for the split-O1-site model are shown in Fig. 10 for both 300 and 15 K. Note that R_w decreases sharply in both cases as $r_{\max}$ is increased for both temperatures. At 300 K R_w reaches an approximately constant value beyond $r_{\max} \sim 10-12$ Å, while at 15 K R_w appears to be constant above $r_{\max} \sim 8-10$ Å. Both results suggest that the disorder in this material extends to at least 8 Å, which is beyond the nearest-neighbor distance range.

D. Spin-dimer analysis

It is clearly of great interest to compare the implications of the disorder models investigated here with the criteria of Saunders and Chalker[20] for the emergence of the spin-glass ground state due to weak disorder in a pyrochlore lattice. A computational estimation of relative strengths of spin inter-

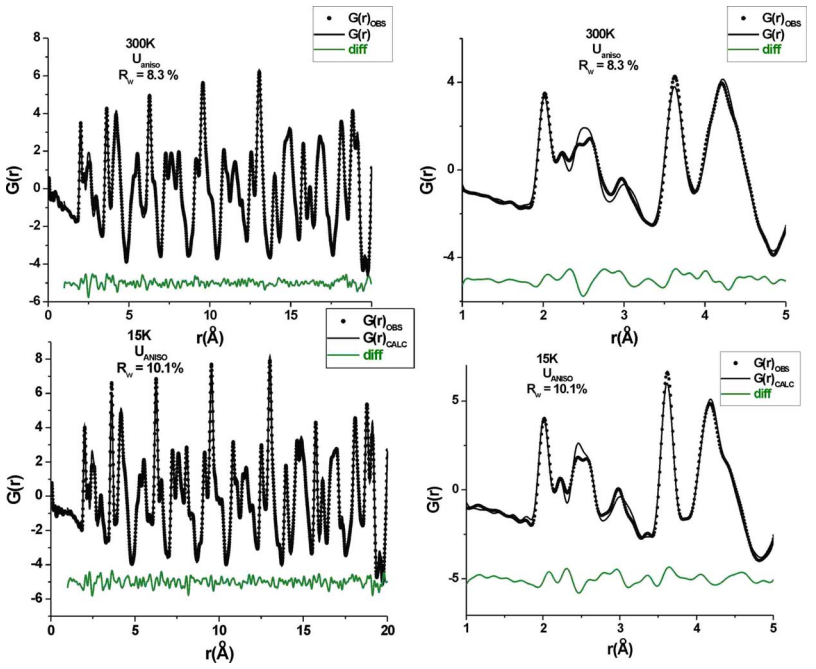

FIG. 7. (Color online) Fits to the $G(r)$ at 300 and 15 K for the fully ordered model with anisotropic ADF for all atoms. Top: 300 K; bottom: 15 K. Left: 0–20 Å; right: 1–5 Å.

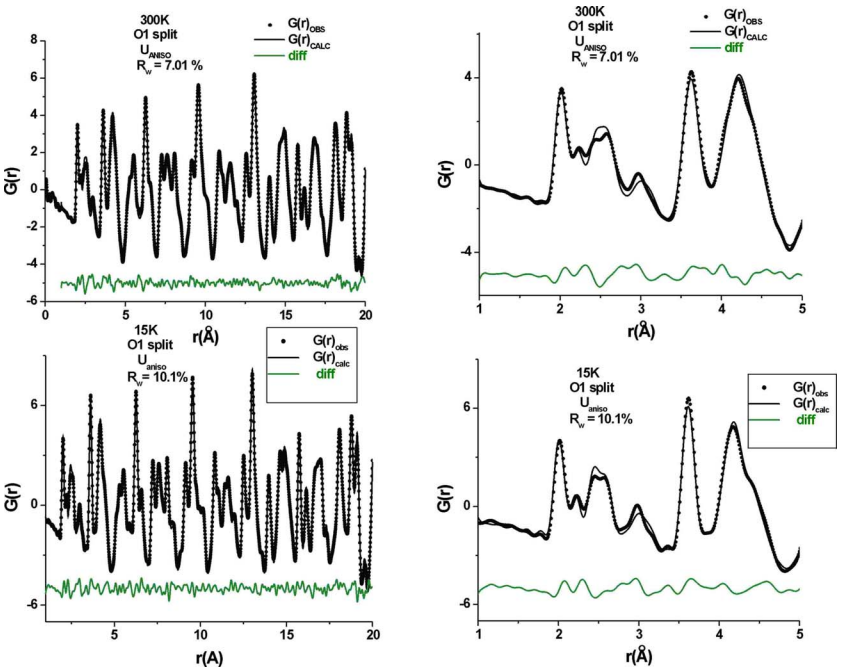

FIG. 8. (Color online) Fits to the $G(r)$ at 300 and 15 K: the split-O1-site model with anisotropic ADF. Top: 300 K; bottom: 15 K. Left: 0–20 Å; right: 1–5 Å.

actions among different magnetic ions and through different pathways was obtained using extended Hückel spin-dimer analysis.[33] The strengths of spin interaction manifested in the exchange constant J are related to the hopping energies among different magnetic sites, Δe, as well as the electron correlation energy U resulting from accommodation of two electrons within the same orbital. These quantities are related through the formula

$$J = -2\frac{(\Delta e)^2}{U}. \quad (1)$$

When comparing J values of different interaction pathways involving the same magnetic ion, the correlation energy, U, is constant and therefore the difference in the $(\Delta e)^2$ value determines the significance of a particular spin interaction relative to the other possible pathways. In these computations three different interaction pathways between two nearest-neighbor Mo sites were considered based on the x positional value for O1 for the average structure and the two extreme values for the split-site model. The values of the intersite hopping energies Δe were acquired by employing the CAESAR package[34] assuming that all three t_{2g} Mo $4d$ orbitals contributed equally to the superexchange interaction. The variation in the Mo-O1-Mo angle and $(\Delta e)^2$ as a function of x is shown in Table VI.

It is clear from Table VI that $\langle \Delta e \rangle^2$ and, thus J, are strong functions of x(O1) and that disorder at this level will lead to a large distribution of exchange constant values, ΔJ, with $\Delta J/J > 0.1$. Thus, in the Saunders-Chalker context it seems clear that a spin-glass ground state for $Y_2Mo_2O_7$ can be understood.

IV. SUMMARY AND CONCLUSIONS

The main conclusions from this work pertinent to the average structure of $Y_2Mo_2O_7$ are that: (1) neutron diffraction data of relatively high resolution can be fitted very well by a fully ordered model with anisotropic ADFs, but (2) the ADFs are indeed highly anisotropic in comparison to isostructural $Y_2Sn_2O_7$, and (3) there is no evidence for a true crystallographic phase transition over the range of 300–15 K within the resolution of the data.

Conclusions relevant to the local structure are that: (1) there is significant disorder associated with the Y-O1 pairs which would be qualitatively consistent with ^{89}Y NMR results reported previously, (2) there is no evidence for a disorder model involving the Mo-Mo pairs proposed previously from EXAFS data, (3) either a dynamic disorder model (anisotropic ADFs) or a static split-O1-site model results in dramatic improvements in fits of the $G(r)$, (4) fits of the local

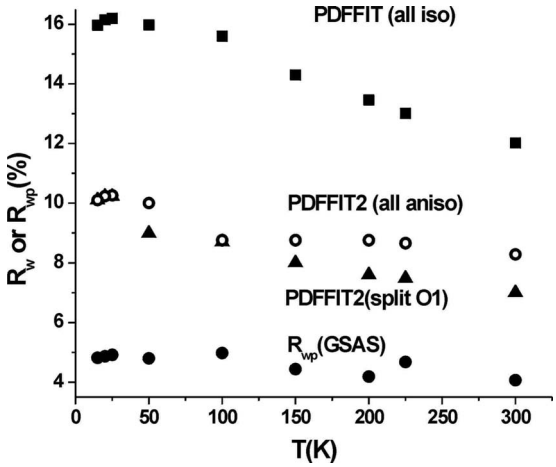

FIG. 9. The evolution of agreement indices R_w and R_{wp} for various models as a function of temperature. R_{wp} (GSAS) refers to the average structure fit of the diffraction data. PDFFIT2(split O1), PDFFIT2(all aniso), and PDFFIT(all iso) correspond to the three models tried for the local structure. Below 50 K the R_w values for the (split O1) and (all aniso) models are numerically the same.

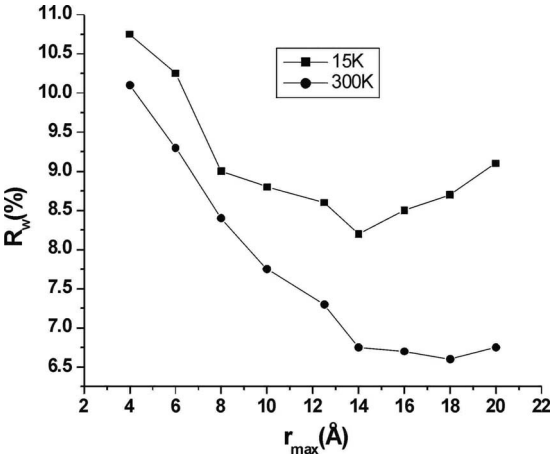

FIG. 10. Comparison of the agreement index R_w as a function of increasing r_{max} with $r_{min}=1$ Å for 30 and 15 K.

structure always become worse as the temperature is decreased for any model, and (5) the range of the disorder extends to 8–12 Å, well beyond nearest neighbors.

The present results are also consistent with the observed spin-glass ground state. In either the static or dynamic disorder model, there is a significant variation in the parameters which determine the nearest-neighbor superexchange interaction in $Y_2Mo_2O_7$ as shown by application of the simple spin-dimer model. While not quantitatively accurate, this model is generally reliable in assessing relative changes. The conclusion here is that the criterion of Saunders and Chalker[20] would appear to be satisfied quantitatively for $Y_2Mo_2O_7$.

To conclude, at least three further questions should be addressed. First, is there genuine static disorder in $Y_2Mo_2O_7$ or large-amplitude dynamic disorder? Both models provide an improved fit to the $G(r)$, with the split-site model being slightly better at high temperatures, albeit with the advantage of three additional free parameters. However, both models appear to give equivalent fits at low temperature. Thus, the NPDF analysis does not provide a clear basis for choice. This situation has elements similar to the well-studied case of the β-cristobalite form of SiO_2 which has been conveniently summarized.[35] β-cristobalite is a high-temperature quenchable form of silica and, coincidentally, crystallizes in $Fd3m$. In the fully ordered model, Si is in 8*a* and O is in 16*c*. However, this requires an unusually short Si-O bond length and a linear Si-O-Si bond angle, which is considered somewhat unlikely. The displacements for the O site are large and anisotropic as well. Early alternative models involved disordering O over the 96 *h* sites with partial occupancy.[36] Refinements of this model led to a six-domain hypothesis with lower tetragonal symmetry and equal distribution of the domains to recover the $Fd3m$ symmetry. This interpretation has been questioned and molecular-dynamics simulations along with inelastic-neutron-scattering, Raman, and infrared data appear to rule out a static disorder model and support a dynamic disorder alternative.[35] Nonetheless, ND data for $Y_2Mo_2O_7$, specifically the very weak variation in the ADFs for O1 and Mo with temperature, suggest strongly the presence of a static component to the disorder. At the very least

TABLE VI. The variation in Mo-O1-Mo angle and $\langle \Delta e \rangle^2$ with $\times$ for O1 in $Y_2Mo_2O_7$.

x(O1)	Mo-O1-Mo (deg)	$\langle \Delta e \rangle^2$ (meV)^2
0.3289	131.9	23579
0.3384	126.9	14212
0.3466	122.7	10546

the data are consistent with a very flat and probably anharmonic potential for the Y-O1 atom pairs. At this stage it is not yet possible to refine anharmonic ADFs within the existing PDFFIT codes. Thus, as the true situation for $Y_2Mo_2O_7$ remains elusive, new data from inelastic-neutron-scattering, Raman, and infrared spectroscopies would be very helpful in resolving this question.

Second, is there any evidence that geometric magnetic frustration plays a causal role in the structural disorder found in this material? At first glance the answer would appear to be no. Data at 300 K indicate that disorder exists in both the average and local structures even at this relatively high temperature. However, fits to the local structure, regardless of model, become significantly worse as the temperature is decreased. For the most realistic local structure models, seemingly discontinuous changes in R_w occur below the range of 100–50 K. Thus, it is impossible to rule out some rather subtle role for magnetic frustration but a detailed model for this is certainly not obvious.

Third and finally, the structures, both average and local, of very few pyrochlore oxides have been studied at the depth presented here. Is local disorder of the type found for $Y_2Mo_2O_7$ commonplace among pyrochlore oxides or is the rare-earth molybdate series unique? That most magnetic pyrochlore materials do not exhibit spin-glass behavior would seem to argue for the latter, but in fact the knowledge base here is very shallow and more work would appear to be warranted.

ACKNOWLEDGMENTS

J.E.G. thanks the Natural Sciences and Engineering Research Council of Canada for support through a Discovery Grant. A.D.L.-G. thanks the Spanish Ministry of Education for support. The authors thank I. P. Swainson for helpful discussions. This work benefited from the use of NPDF at the Lujan Center at Los Alamos Neutron Science Center, funded by DOE Office of Basic Energy Sciences. Los Alamos National Laboratory is operated by Los Alamos National Security LLC under DOE Contract No. DE-AC52-06NA25396. The upgrade of NPDF was funded by NSF through Grant No. DMR 00-76488. Work by the Billinge group was supported by the Office of Science, U.S. Department of Energy, under Contract No. DE-AC02-98CH10886.

[1] J. S. Gardner, M. J. P. Gingras, and J. E. Greedan, Rev. Mod. Phys. (to be published).
[2] J. E. Greedan, M. Sato, Xu Yan, and F. S. Razavi, Solid State Commun. **59**, 895 (1986).
[3] P. H. Hubert, Bull. Soc. Chim. Fr. **11**, 2385 (1974).
[4] P. H. Hubert, Bull. Soc. Chim. Fr. **111**, 2463 (1975).
[5] M. J. P. Gingras, C. V. Stager, N. P. Raju, B. D. Gaulin, and J. E. Greedan, Phys. Rev. Lett. **78**, 947 (1997).
[6] J. S. Gardner, B. D. Gaulin, S.-H. Lee, C. Broholm, N. P. Raju, and J. E. Greedan, Phys. Rev. Lett. **83**, 211 (1999).
[7] N. P. Raju, E. Gmelin, and R. K. Kremer, Phys. Rev. B **46**, 5405 (1992).
[8] S. R. Dunsiger, R. F. Kiefl, K. H. Chow, B. D. Gaulin, M. J. P. Gingras, J. E. Greedan, A. Keren, K. Kojima, G. M. Luke, W. A. MacFarlane, N. P. Raju, J. E. Sonier, Y. J. Uemura, and W. D. Wu, Phys. Rev. B **54**, 9019 (1996).
[9] K. Miyoshi, Y. Nishimura, K. Honda, K. Fujiwara, and J. Takeuchi, J. Phys. Soc. Jpn. **69**, 3517 (2000).
[10] J. S. Gardner, G. Ehlers, R. H. Heffner, and F. Mezei, J. Magn. Magn. Mater. **226-230**, 460 (2001).
[11] J. S. Gardner, G. Ehlers, S. T. Bramwell, and B. D. Gaulin, J. Phys.: Condens. Matter **16**, S643 (2004).
[12] F. C. Montenegro, S. M. Rezende, and M. D. Coutinho-Fihlo, J. Appl. Phys. **63**, 3755 (1988).
[13] H. Kato, K. Iwai, A. Ito, and Y. Nakagawa, J. Magn. Magn. Mater. **140-144**, 1801 (1995).
[14] K. Binder, W. Kinzel, H. Maletta, and D. Stauffer, J. Magn. Magn. Mater. **15-18**, 189 (1980).
[15] M. A. Subramanian and A. W. Sleight, in *Handbook on the Physics and Chemistry of Rare Earths*, edited by K. A. Gschneidner, Jr. and L. Eyring (Elsevier Science, New York, 1993), Vol. 16, p. 225.
[16] J. N. Reimers, J. E. Greedan, and M. Sato, J. Solid State Chem. **72**, 390 (1988).
[17] L. Minervini, R. Grimes, Y. Tabira, R. L. Withers, and K. Sickafus, Philos. Mag. A **82**, 123 (2002).
[18] W. Ratcliff, S. H. Lee, C. Broholm, S. W. Cheong, and Q. Huang, Phys. Rev. B **65**, 220406(R) (2002).
[19] R. D. Shannon, Acta Crystallogr., Sect. A: Cryst. Phys., Diffr., Theor. Gen. Crystallogr. **32**, 751 (1976).
[20] T. E. Saunders and J. T. Chalker, Phys. Rev. Lett. **98**, 157201 (2007).
[21] C. H. Booth, J. S. Gardner, G. H. Kwei, R. H. Heffner, F. Bridges, and M. A. Subramanian, Phys. Rev. B **62**, R755 (2000).
[22] A. Keren and J. S. Gardner, Phys. Rev. Lett. **87**, 177201 (2001).
[23] E. Sagi, O. Ofer, A. Keren, and J. S. Gardner, Phys. Rev. Lett. **94**, 237202 (2005).
[24] J. A. Hodges, P. Bonville, A. Forget, J. P. Sanchez, P. Vulliet, M. Rams, and K. Krolas, Eur. Phys. J. B **33**, 173 (2003).
[25] S. J. L. Billinge, Z. Kristallogr. **219**, 117 (2004).
[26] T. Proffen, T. Egami, S. J. L. Billinge, A. K. Cheetham, D. Loluca, and J. Parise, Appl. Phys. A: Mater. Sci. Process. **74**, S163 (2002).
[27] C. L. Farrow, P. Juhas, J. W. Liu, D. Bryndin, E. S. Bozin, J. Bloch, Th. Proffen, and S. J. L. Billinge, J. Phys.: Condens. Matter **19**, 335219 (2007).
[28] M. Sato, Xu Yan, and J. E. Greedan, Z. Anorg. Allg. Chem. **540**, 177 (1986).
[29] B. J. Kennedy, B. A. Hunter, and C. J. Howard, J. Solid State Chem. **130**, 58 (1997).
[30] T. Birchall and A. W. Sleight, J. Solid State Chem. **13**, 118 (1975).
[31] A. L. Hector and S. B. Wiggin, J. Solid State Chem. **177**, 139 (2004).
[32] T. Egami and S. J. L. Billinge, *Underneath the Bragg Peaks: Structural Analysis of Complex Materials* (Plenum, Oxford, 2003).
[33] M. H. Whangbo, H. J. Koo, and D. J. Dai, J. Solid State Chem. **176**, 417 (2003).
[34] J. Ren, W. Liang, and M. H. Whangbo, Crystal and Electronic Structure Analysis Using CAESAR, 2005 (http://www.primeC.com).
[35] I. P. Swainson and M. T. Dove, J. Phys.: Condens. Matter **7**, 1771 (1995).
[36] D. M. Hatch and M. Ghose, Phys. Chem. Miner. **17**, 554 (1991); A. F. Wright and A. J. Leadbetter, Philos. Mag. **31**, 1391 (1975).